

## Effects of GlyT1 inhibition on erythropoiesis and iron homeostasis in rats

Michael Winter<sup>a</sup>, Jürgen Funk<sup>a</sup>, Annette Körner<sup>a</sup>, Daniela Alberati<sup>b</sup>, Francois Christen<sup>a</sup>, Georg Schmitt<sup>a</sup>, Bernd Altmann<sup>a</sup>, Andreas Pospischi<sup>c</sup>, and Thomas Singer<sup>a</sup>

<sup>a</sup>Pharmaceutical Research and Early Development, Pharmaceutical Sciences, Roche Innovation Center Basel, F. Hoffmann-La Roche, Basel, Switzerland; <sup>b</sup>Pharmaceutical Research and Early Development, Neuroscience Discovery, Roche Innovation Center Basel, F. Hoffmann-La Roche, Basel, Switzerland; <sup>c</sup>Institute of Veterinary Pathology, Vetsuisse-Faculty, University Zurich, Switzerland

(Received 3 May 2016; revised 28 June 2016; accepted 29 June 2016)

---

Glycine is a key rate-limiting component of heme biosynthesis in erythropoietic cells, where the high intracellular glycine demand is primarily supplied by the glycine transporter 1 (GlyT1). The impact of intracellular glycine restriction after GlyT1 inhibition on hematopoiesis and iron regulation is not well established. We investigated the effects of a potent and selective inhibitor of GlyT1, bitopertin, on erythropoiesis and iron homeostasis in rats. GlyT1 inhibition significantly affected erythroid heme biosynthesis, manifesting as microcytic hypochromic regenerative anemia with a 20% steady-state reduction in hemoglobin. Reduced erythropoietic iron utilization was characterized by down-regulation of the transferrin receptor 1 (TfR1) on reticulocytes and modest increased iron storage in the spleen. Hepatic hepcidin expression was not affected. However, under the condition of reduced heme biosynthesis with reduced iron reutilization and increased storage iron, hepcidin at the lower and higher range of normal showed a striking role in tissue distribution of iron. Rapid formation of iron-positive inclusion bodies (IBs) was observed in circulating reticulocytes, with an ultrastructure of iron-containing polymorphic mitochondrial remnants. IB or mitochondrial iron accumulation was absent in bone marrow erythroblasts. In conclusion, GlyT1 inhibition in rats induced a steady-state microcytic hypochromic regenerative anemia and a species-specific accumulation of uncommitted mitochondrial iron in reticulocytes. Importantly, this glycine-restricted anemia provides no feedback signal for increased systemic iron acquisition and the effects reported are pathogenetically distinct from systemic iron-overload anemias and erythropoietic disorders such as acquired sideroblastic anemia. Copyright © 2016 Published by Elsevier Inc. on behalf of ISEH - International Society for Experimental Hematology.

---

The glycine transporter 1 (GlyT1) was originally identified as a member of the solute carrier family 6 of sodium- and chloride-dependent neurotransmitter transporters [1]. GlyT1 is expressed in the central nervous system and in peripheral tissues; mainly in erythroid cells, from erythroblasts in the bone marrow up to circulating reticulocytes in humans [2] and rats [3]. Reduced glycine transfer may affect hemoglobin (Hb) biosynthesis because glycine is a key rate-limiting component in the first catalytic reaction of the heme synthesis pathway.

---

Offprint request to: Michael Winter, Roche Pharmaceutical Research and Early Development, Pharmaceutical Sciences, Roche Innovation Center Basel, Bldg. 73-216b, CH-4070 Basel, Switzerland; E-mail: [michael.winter@roche.com](mailto:michael.winter@roche.com)

Supplementary data related to this article can be found at <http://dx.doi.org/10.1016/j.exphem.2016.07.003>.

Heme biosynthesis begins and ends in the mitochondria, involves eight enzymatic reactions, and is highly conserved in mammals [4]. It is initiated with a condensation reaction between glycine and succinyl coenzyme A to form 5-aminolevulinic acid (ALA). ALA is catalyzed by  $\delta$ -aminolevulinic acid synthase 2 (ALAS2) in erythroid cells. ALAS2 expression is controlled by erythroid-specific transcription factors that adjust the rate of heme synthesis based on intracellular iron availability [5]. In the final reaction, heme is formed by ferrochelatase catalyzing the insertion of a ferrous iron into a protoporphyrin IX (PPIX) ring. Heme is then exported out of the mitochondria to associate with globin chains and apocytochromes, a process mediated by adenosine triphosphate (ATP)-binding cassette transporters, forming Hb [6].

In vitro studies suggest that GlyT1 is no longer expressed in mature red blood cells (RBCs), limiting its function to erythrocyte precursors including reticulocytes [3].

Reticulocytes continue to produce Hb for a short period in bone marrow and peripheral circulation using residual ribosomal RNA [7,8]. Although GlyT1 has been shown to be the main contributor to glycine uptake in reticulocytes, accounting for 42% of glycine uptake in humans [9], the remaining glycine transfer occurs via other, less specific transporters. GlyT1 inhibition is thus not anticipated to cause complete glycine deficiency in pre-erythrocytes, which is supported by our dataset presented.

Disorders of erythropoiesis are often associated with abnormal iron homeostasis [10]. Although regulatory feedback mechanisms of reduced heme biosynthesis at inadequately low availability of iron are well understood, less is known about the impact of glycine restriction on hematopoiesis and iron regulation. The aim of this mechanistic study was to determine the effects of GlyT1 inhibition on erythropoiesis and iron homeostasis in rats using bitopertin (RG1678), a potent, selective, and reversible inhibitor of GlyT1 that has been well characterized in preclinical studies [11,12].

## Materials and methods

### *Animals and husbandry*

Because female rats showed higher oral bioavailability for bitopertin than males, only female rats were used in this study. Female Wistar rats (substrain: HanRCCWIST [SPF], Harlan Laboratories, Ltd., Horst, The Netherlands), approximately 16 weeks of age, were acclimatized for 5–13 days and housed in pairs in environmentally enriched Macrolon boxes at a temperature of 20–24°C, with 40–80% humidity and a 12-hour light/dark cycle. A pelleted (gavage administration) or powdered (dietary administration) diet and tap water were supplied ad libitum.

### *Study design and procedures*

Daily doses of vehicle or bitopertin suspensions were administered by oral gavage (vehicle, 1, 3, or 8 mg/kg) or admixed in a powdered diet at equivalent exposure doses (vehicle, 1, 3, or 15 mg/kg) over a period of 58 or 59 days. Animals receiving 15 mg/kg initially received 10 mg/kg/day in week 1 to increase tolerability. Each dose group consisted of 28 rats, 14 dosed by oral gavage and 14 by diet admix, to assess the effects of distinct exposure profiles. Because no differences in the dose–response effects were observed, results were merged and presented by dose groups.

Necropsies were performed on 16 animals from each dose group at the end of the treatment period on day 60. The remaining recovery animals ( $n = 12$ ) were sacrificed at the end of a 4-week treatment-free period, on day 88. Animals were killed by CO<sub>2</sub> inhalation and exsanguination, and all major organs and tissues were collected.

Two additional long-term studies were conducted as part of the preclinical safety program of bitopertin. Pivotal hematology, blood smear morphology, and histopathology findings of iron-sensitive organs and tissues are reported from these studies to demonstrate the long-term consistency of findings (Supplementary Methods, online only, available at [www.exphem.org](http://www.exphem.org)).

All studies were performed in laboratories approved by the Association for the Assessment and Accreditation of Laboratory Animal Care and were carried out in accordance with the European Union Directive 2010/63/EU for animal experiments.

### *Hematology parameters, clinical chemistry, and iron biomarkers*

Nonfasting blood samples were drawn under light isoflurane anesthesia before dosing in week 1 (day 2 [gavage] or day 3 [diet admix]), week 2 (day 10), week 4 (days 24 and 25), at the end of the treatment period (days 58 and 59), and at the end of the recovery period (day 88). Hematological parameters were measured using a hematology analyzer (Sysmex XT, Sysmex, Kobe, Japan).

Serum total iron-binding capacity and serum iron were measured using an ADVIA 1650 (Siemens, Tarrytown, NY). Serum ferritin and transferrin were measured with commercial enzyme-linked immunosorbent assays (ELISAs; E-25F, Immunology Consultants Laboratory, Inc., Portland, OR) and MBS564129 (MyBioSource, Inc., San Diego, CA), respectively. Transferrin saturation was calculated as the ratio of serum iron and total iron-binding capacity multiplied by 100. Total free erythrocyte PPIX was determined using a fluorescence photometry assay as described by Piomelli et al. [13]. ELISA and PPIX assays were analyzed on a SpectraMax microplate reader with SoftMax Pro software (Molecular Devices, LLC, Sunnyvale, CA). Serum erythropoietin (EPO) concentrations were determined with an immunoassay on the Gyrolab® instrument (Gyros AB, Uppsala, Sweden) with antibody reagents from R&D Systems (Minneapolis, MN): rat EPO-specific biotinylated capture antibody BAM9592 and MAB9591 conjugated to Alexa Fluor® 647 with the monoclonal antibody labeling kit (Molecular Probes, Eugene, OR). EPO concentrations in samples were calculated by the Gyrolab Evaluator software, version 3.15.137 (from a recombinant rat EPO standard curve [1306-RE-010/CF, R&D Systems]).

### *Blood and bone marrow smears*

Blood smears were stained with Wright–Giemsa stain for examination of RBC morphology and inclusion bodies (IBs) and scored as follows: 0 = no IB; 1 = few IB-positive reticulocytes, absence in RBC; 2 = most reticulocytes IB positive, few/no RBC affected; 3 = most reticulocytes IB positive, moderate incidence in RBC; 4 = most reticulocytes positive, marked incidence in RBC; and 5 = absence of IB in reticulocytes, marked incidence in RBC. Blood smears were also stained with Perls' stain for identification of iron-positive IB.

Bone marrow smears from all animals at the end of treatment were stained with Perls' stain for identification of siderotic granules in erythroblasts according to the scoring system reported in Mufti et al. [14].

### *Histopathology*

Spleen, pancreas and liver tissues were fixed in 10% formalin and embedded in paraffin from which slides were prepared and stained with hematoxylin–eosin and Perls' stain and examined under a light microscope. For iron scoring in the spleen and liver, the following scores were applied: 0 = none; 1 = minimal (approximately 1–20% of macrophages or Kupffer cells/hepatocytes affected); 2 = slight (approximately 21–40% of cells affected); 3 = moderate (approximately 41–60% of cells

affected); 4 = marked (61–80% of cells affected); and 5 = severe (approximately 81–100% of cells affected). Automated image analysis of spleen iron was also performed ([Supplementary Methods](#)).

#### *Electron microscopy*

RBC from selected high-dose (8 or 15 mg/kg) and control animals were fixed in glutaraldehyde, osmicated, and embedded in resin. Semi-thin sections were stained with toluidine blue. Areas suitable for examination were selected using a light microscope and then microtomed to create ultra-thin sections, which were contrasted using uranyl acetate and lead citrate and examined using an electron microscope (CM10, Philips Electron Instruments, Eindhoven, The Netherlands).

#### *CD71 (TfR-1) expression on reticulocytes by flow cytometry*

Cell surface CD71 expression on reticulocytes was determined with phycoerythrin-labeled anti-rat CD71 monoclonal antibody (BD-Pharmingen™, San Diego, CA) on thiazole-orange-positive reticulocytes (Retic-COUNT™ reagent, BD Biosciences, San Jose, CA) on a Cytomics FC 500 MPL flow cytometer with MXP software version 2.1 (Beckman Coulter®, Miami, FL). Fluorescence intensity binding signals were normalized to antibody-binding capacity units with the Quantum™ Simply Cellular® anti-rat IgG beads using the QuickCal software version 2.3 (Bangs Laboratories, Inc., Fishers, IN).

#### *HAMP expression in the liver by in situ hybridization*

Hepcidin antimicrobial peptide (HAMP) mRNA was detected in rat liver samples using RNAscopeVS® (Advanced Cell Diagnostics, Inc., Hayward, CA), an RNA in situ hybridization (ISH) method that permits signal amplification and background suppression (for details, see the [Supplementary Methods](#)).

#### *Statistical analysis*

Group means and standard deviations (SDs) for hematological parameters and serum biomarkers were calculated for  $n \geq 3$  animals per group using Proventus software (Instem Life Sciences, Stone, UK). Differences between the control group and treated groups were determined using an ANOVA and Dunnett's multiple-comparisons test and are indicated by significances of  $*p < 0.05$ ,  $**p < 0.01$ , and  $***p < 0.001$ .  $p < 0.05$  was considered statistically significant.

## Results

### *GlyT1 inhibition causes microcytic hypochromic regenerative anemia in rats*

Reduced erythrocyte mean corpuscular Hb (MCH) was observed in all rats treated with bitopertin. Ret-Y (a marker for reticulocyte Hb) [15] showed a significant early (days 2/3) decrease in treated compared with control animals, almost plateaued at about  $-25\%$  by day 10, and remained low until the end of the treatment period with a weak dose-dependent effect ([Fig. 1A](#)). MCH and mean corpuscular volume (MCV) showed a slow but progressive decline from day 10 to the end of the treatment of about  $-25\%$  and  $-20\%$ , respectively ([Fig. 1B and C](#)).

Compensatory reticulocytosis and erythrocytosis were observed under GlyT1 inhibition, with a mean erythrocyte count increase of approximately 10% starting on days 24/25 until the end of treatment ([Fig. 1D](#)). Despite this compensatory regeneration, hematocrit (Hct, data not shown) and mean Hb ([Fig. 1E](#)) decreased progressively by approximately 20% from day 3 to the end of treatment. A mild increase in thrombocytes was also seen in all treated rats. A modest, dose-proportional increase in mean group serum EPO concentration was observed from day 10 until the end of the treatment period, further indicating an EPO-responsive anemia ([Fig. 1F](#)).

After discontinuation of treatment, Ret-Y values returned to control group levels at the end of the recovery period (day 88). However, mean MCH, Hb, Hct (data not shown), and erythrocyte counts did not reach complete normalization. EPO returned to control levels ([Fig. 1F](#)).

Long-term effects on erythropoiesis beyond multiples of a rat RBC lifespan were shown in two rat studies with bitopertin exposure of up to 2 years. The results were consistent with the pivotal 8-week mechanistic study and demonstrated a steady-state microcytic hypochromic erythropoiesis, with MCH and Hb reductions of approximately 20% associated with elevated erythrocyte counts ([Supplementary Figure E1](#), online only, available at [www.exphem.org](http://www.exphem.org)).

### *GlyT1 inhibition induces iron-containing inclusion bodies in rats, but not type III ring sideroblasts*

Rapid development of basophilic IB was detected early on Wright–Giemsa-stained blood smears, with IBs present in most reticulocytes in all treated dose groups at day 2. IBs were subsequently found in a few erythrocytes in all dose groups at day 10 and a dose-dependent effect on IBs was observed at the end of the treatment period. No IBs were detected on day 88, suggesting complete normalization during the 28-day recovery period ([Fig. 2](#)). Chronic GlyT1 inhibition in a long-term 2-year study resulted in only a minimal increase in IBs between 6 months and 1 year and remained stable until the end of the 2-year treatment.

IBs that had a basophilic polymorphic structure on Wright–Giemsa stains ([Fig. 3A and B](#)), were shown to be iron-positive with Perls' stain ([Fig. 3D](#)), and were accompanied by a pronounced poikilocytosis of a schistocyte-like cell morphology ([Fig. 3B](#)). Hypochromic microcytic erythrocytes and irregularly shaped RBCs (poikilocytes) remained at the end of the recovery period, but IBs were entirely absent. Examination of bone marrow smears of treated rats at the end of the treatment period revealed an unremarkable erythroblast cell phenotype with no evidence of pathological ring sideroblasts (Type III) ([Fig. 3E and F](#)). A few type I and II sideroblasts were observed as single cells in individual blood smears of control and treated rats.

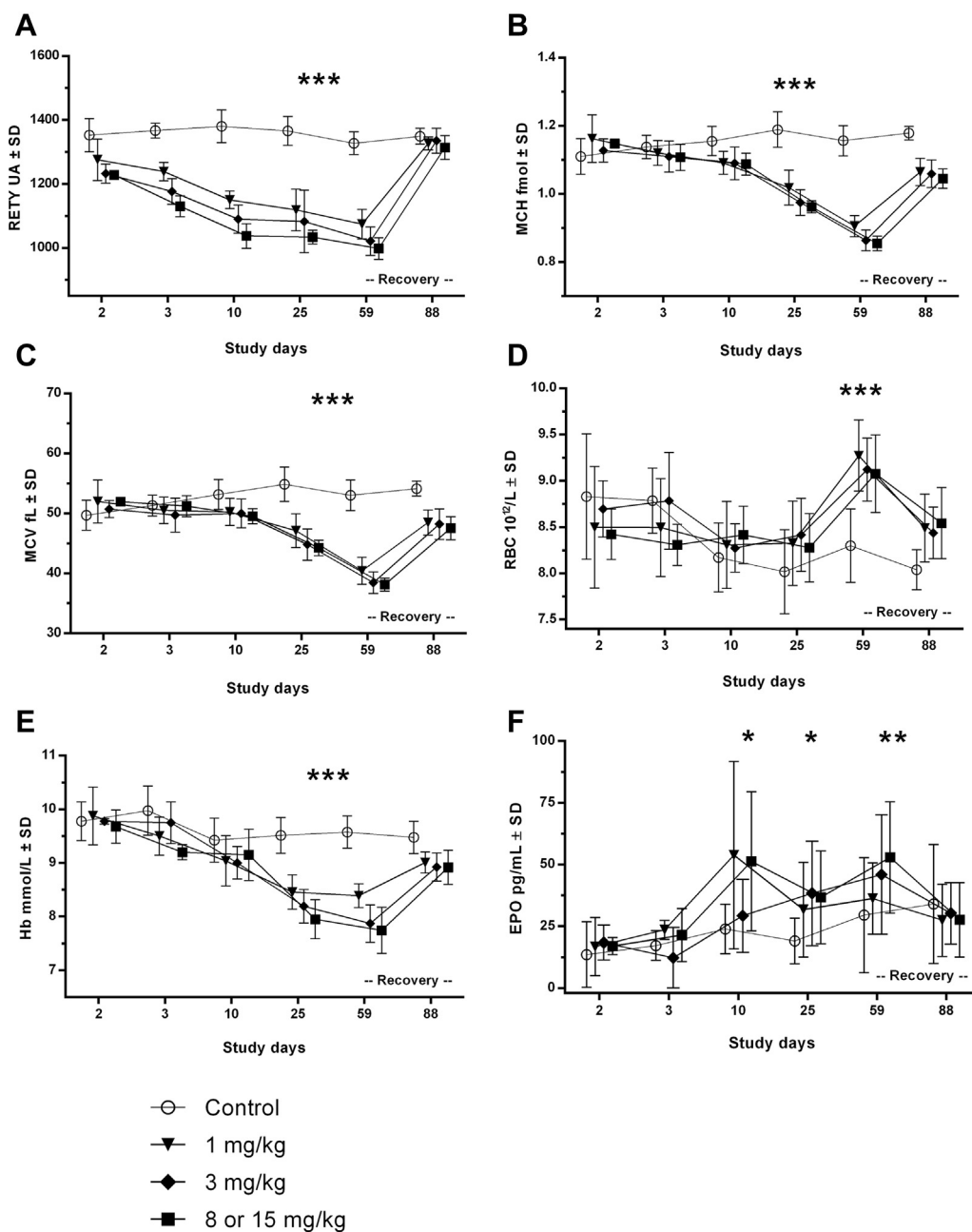


**Figure 1.** Changes in hematological parameters characteristic of microcytic hypochromic regenerative anemia. GlyT1 inhibition causes reduced reticulocyte and erythrocyte hemoglobinization, compensatory erythrocytosis, and reduced Hb, all characteristic for microcytic hypochromic anemia. The increase in mean group serum EPO concentration indicates an EPO-responsive anemia. Hematology parameters (mean  $\pm$  SD) by bitopertin dose group measured on day 2 (gavage dosed subgroup;  $n = 4$ ), day 3 (diet admix subgroup;  $n = 4$ ), day 10 (data combined;  $n = 8$ ), days 24/25 (data combined;  $n = 16$ ), at the end of the treatment period (days 58/59, data combined;  $n = 16$ ), and at the end of the recovery period (day 88, data combined;  $n = 12$ ) are shown for Ret-Y (A), MCH (B), MCV (C), RBC count (D), Hb (E), and EPO (F). \* $p < 0.05$ , \*\* $p < 0.01$ , and \*\*\* $p < 0.001$  in treated groups compared with controls.

Electron microscopy examination of RBCs showed IBs with a distinct morphology in treated animals compared with the iron-containing vesicles seen typically in reticulocytes. These IBs were polymorphic, irregularly shaped or round to oval, membrane bound, and filled with remnants of mitochondrial cristae and iron micelles. Consistent with the distribution in blood

smears, polymorphic IBs were predominantly found in reticulocytes (Fig. 3G–I).

*Effects of GlyT1 inhibition on iron storage and availability in the hematopoietic system*

Mean serum ferritin levels showed a modest time- and dose-independent increase in treated compared with control

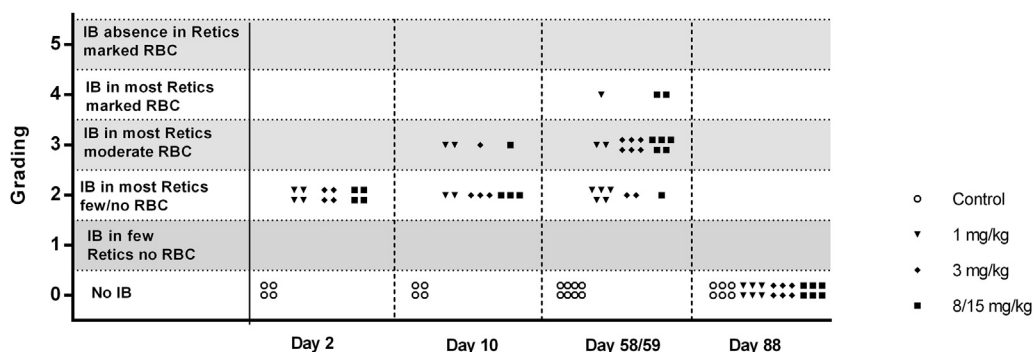


**Figure 2.** IB grading by dose group (gavage) over the duration of the study. GlyT1 inhibition induced a rapid development of IBs, with IBs present in most reticulocytes already at day 2 of all treated dose groups, which was followed by a moderate progression in severity at later time points and full reversibility within a 4-week recovery period. Typical IB grading from Wright–Giemsa-stained blood films are presented from the bitopertin-gavage-dosed subgroups because early day 2 samples were taken in this subgroup only. Sampling was done on days 2 ( $n = 4$ ), 10 ( $n = 4$ ), 58/59 ( $n = 8$ ), and 88 ( $n = 6$ ). Feed–admix-dosed animals showed nearly identical results (data not shown).

rats. In treated rats, mean serum ferritin levels decreased below control group levels at the end of the recovery period, indicating efficient iron reutilization after restoration of normal heme biosynthesis. Remarkably, a marked increase in serum ferritin was noted in a few control group animals and was responsible at the end of the treatment and recovery phases for the high mean group variability (Fig. 4).

To determine the effect of GlyT1 inhibition on functional iron availability, flow cytometry was used to measure the expression of the membrane-bound transferrin receptor 1 (TfR-1 or CD71). Two reticulocyte populations expressing CD71 were identified: one with low fluorescence/RNA and low CD71 (TfR-1 LFR) and one with high fluorescence/RNA with high CD71 (TfR-1 HFR) consistent with reticulocyte maturation and CD71 cleavage. A clear trend for reduced expression of CD71 was observed in both reticulocyte populations in treated compared with control rats at the end of the dosing phase, with a maximum reduction of 25% and a statistically significant difference in the LFR reticulocytes (Fig. 5).

A modest but significant increase in total free erythrocyte PPIX was noted from days 24/25 to the end of the treatment period and normalized at the end of the treatment period (Fig. 6).

#### *GlyT1 inhibition does not affect systemic acquisition of iron*

Serum iron, transferrin, and transferrin saturation were all within the control group range. A modest increase in hemosiderin deposits was observed in treated rats compared with controls in the spleen only and insignificantly reversed during the 28-day recovery period due to the relative low bioavailability of hemosiderin iron. The histology grading correlated with quantitative imaging of the iron-stained spleen area, where hemosiderin deposits were statistically significantly increased in all groups at the end of the treatment period (Supplementary Figure E2, online only, avail-

able at [www.exphem.org](http://www.exphem.org)). The incidence of animals with hemosiderin deposits in the liver was slightly higher in treated rats, although the severity was within the control group range (Fig. 7). Consistent with iron retention and absence of systemic iron accumulation, chronic exposure to bitopertin (up to 2 years) resulted in a dose-proportional increase in hemosiderin deposition in spleen macrophages only.

GlyT1 inhibition did not affect hepatic expression of hepcidin, with levels observed in bitopertin-treated animals within the control group range at the end of the treatment period (Supplementary Figure E3, online only, available at [www.exphem.org](http://www.exphem.org)). Hepcidin expression in the liver was significantly ( $p = 0.0047$ ) correlated with serum iron concentration, demonstrating that ISH is a sensitive method for measuring serum hepcidin activity (Supplementary Figure E3B, online only, available at [www.exphem.org](http://www.exphem.org)).

Within the observed normal strain-specific variability of hepcidin activity, hepcidin proved to be a strong regulator of iron distribution. Rats with an elevated liver iron score showed low spleen iron deposition at hepcidin expression rates at the lower range of normal. Conversely, hepcidin expression at the higher range of normal was strongly associated with preferential spleen but low liver iron deposition (Fig. 7). High serum ferritin correlated with liver iron deposition, but was insensitive for spleen hemosiderosis (Fig. 8).

## Discussion

In this study, we investigated the role of GlyT1 on erythropoiesis and iron homeostasis in erythrocyte precursors by using bitopertin, a potent and selective inhibitor of GlyT1. We demonstrated that inhibition of GlyT1 disturbed Hb synthesis in rats, which manifested as a regenerative microcytic hypochromic anemia. This effect is clearly target related because microcytic hypochromic anemia with a similar magnitude of effect on MCH

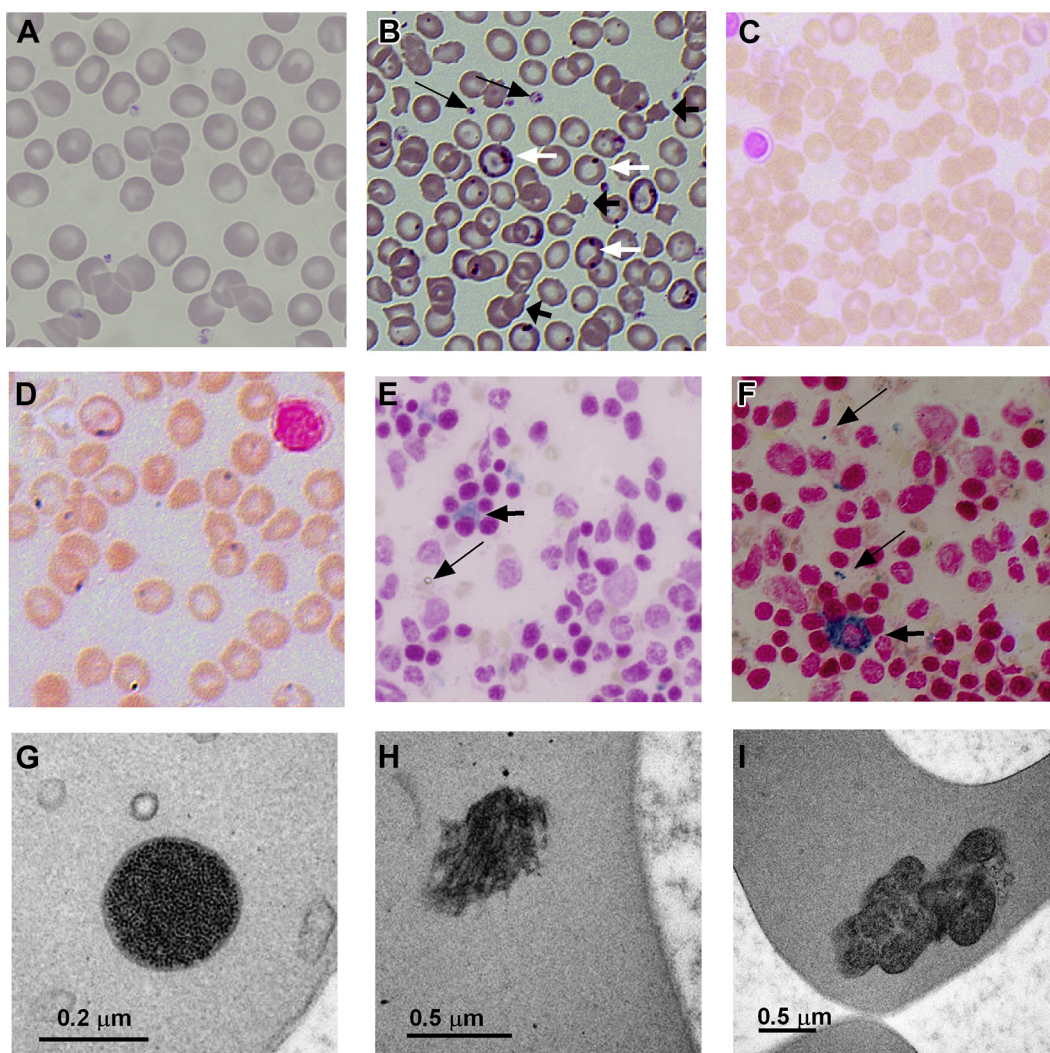


**Figure 3.** IBs and RBC abnormalities noted in blood and bone marrow smears. Representative microphotographs of blood smears taken at the end of the treatment period (days 58/59) from representative rats of the control and the 8/15 mg/kg bitopertin dose group. Blood smears stained with Wright–Giemsa from a control (A) and a treated (B) rat show polychromasia, mild thrombocytosis (long arrows), and poikilocytosis (short arrows). IBs were found predominantly in polychromatophilic erythrocytes (reticulocytes, white arrows) and erythrocytes. Blood smear stained with Perls' stain showing iron-positive IBs in a treated animal (D) and an absence of IBs in controls (C). Bone marrow iron stains with unremarkable erythroblast iron load. Absence of pathological ring sideroblasts (type III) in bone marrow smears stained with Perls' stain illustrated in a treated rat (F) compared with control group bone marrow (E). Black arrowheads indicate an erythron composed of a macrophage with pronounced storage iron surrounded by normal erythroblasts of various maturational stages. Whereas ring sideroblasts were absent, discrete iron-positive IBs were present in reticulocytes in all animals (long arrow), with a trend for a more condensed form and a higher incidence in treated rats. Blood and bone marrow smear images were taken on a Zeiss AxioScope microscope with a  $630 \times 10$  EC Plan Neofluar oil-immersion objective and an Olympus SC30 camera using Olympus analySIS software version 5.1. (G–I) Electron microscopy (Philips CM10 electron microscope) images of reticulocytes. Classic ferric bodies and small, iron-containing vesicular IBs were seen in both control and treated animals. Classic small ferric bodies (diameter approximately  $0.2 \mu\text{m}$ ) were characterized by round inclusions limited by a membrane-like structure and filled with electron-dense granules resembling ferritin particles (G, treated rat). The relatively small, electron-dense vesicular IBs (diameter approximately  $0.5 \mu\text{m}$ ) with electron-dense granules might resemble uncommitted iron precipitation during the final erythrocyte maturation phase (H, control rat). Polymorphic IBs of a significantly larger size (diameter approximately  $1.5 \mu\text{m}$ ), containing iron micelles and representing mitochondrial remnants, were found in reticulocytes of treated rats only (I).

(21% reduction) was reported in  $\text{GlyT1}^{-/-}$  mice [16], indicating a complete inhibition of GlyT1 under the selected experimental conditions.

GlyT1 inhibition also resulted in the rapid development of iron-positive IBs within 24 hours after the first dose in the majority of reticulocytes, with a subsequent minimal

extended manifestation in erythrocytes (siderocytes). Because rat reticulocytes have a bone marrow maturation phase of about 20 hours before release into circulation [17], the rapid onset of IBs strongly suggests that IB formation occurred within this maturation phase in the bone marrow.

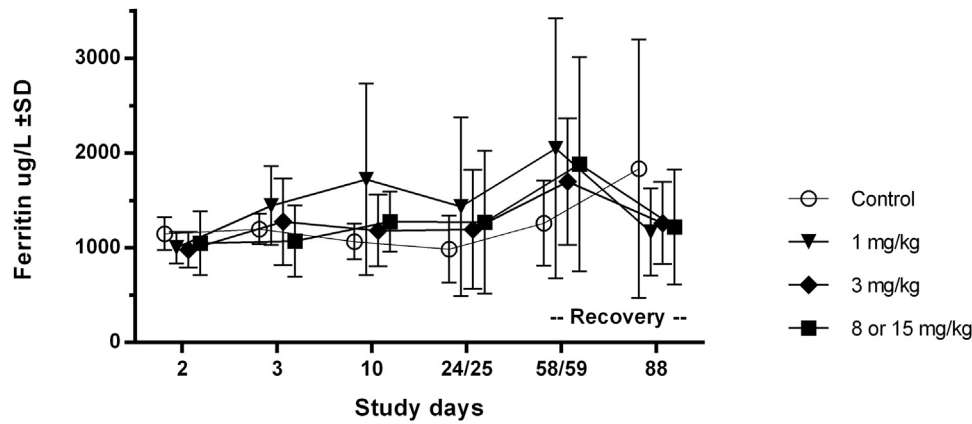


**Figure 4.** GlyT1 inhibition moderately increases serum ferritin levels. Reduction in heme biosynthesis induced by GlyT1 inhibition caused iron retention in the storage pool, as indicated by moderately increased serum ferritin levels. Full restoration of heme synthesis capacity during the recovery period was associated with a rapid reutilization of storage iron and normalization of serum ferritin concentrations. Mean  $\pm$  SD levels of serum ferritin by bitopertin dose group measured on day 2 (gavage dosed subgroup;  $n = 4$ ), day 3 (diet admix subgroup;  $n = 4$ ), day 10 (data combined;  $n = 8$ ), days 24/25 (data combined;  $n = 16$ ), at the end of the treatment period (days 58/59, data combined;  $n = 16$ ), and at the end of the recovery period (day 88, data combined;  $n = 12$ ). Statistical significance between treated and control groups was not reached at any time point due to large interindividual variability.

IBs were electron-microscopically characterized as iron-containing polymorphic mitochondrial remnants, indicating the persistence of uncommitted mitochondrial iron reticulocytes when heme biosynthesis is inhibited. This ultrastructure was comparable to IBs typically found in erythrocytes and erythroblasts of various forms of sideroblastic anemia [18]. In humans, acquired sideroblastic anemia has significant bone marrow involvement [19] and the diagnosis is confirmed by the widespread presence of abnormal ring sideroblasts (type III) in bone marrow samples using light and electron microscopy [20]. Type III sideroblasts were, however, absent in the rat bone marrow.

IBs had a clear vesicular ultrastructure, suggesting that a large part of the iron-containing mitochondrial remnants

might be cleared via normal autophagy processes during final reticulocyte maturation [21]. IB formation was followed by characteristic changes in RBC morphology, with irregularly shaped RBCs and a schistocyte-like cell morphology in a subfraction of erythrocytes. These poikilocytes are thought to be secondary to incomplete autophagic clearance of mitochondrial remnants by the spleen because removal of siderotic bodies from erythrocytes in the spleen is known to result in fragmented RBCs [22], and erythrocytes with siderotic bodies are frequently observed after splenectomy [23,24].

A compensatory downregulation of TfR-1 expression on reticulocytes was shown after GlyT1 inhibition, indicating reduced iron incorporation into erythroblasts and thus

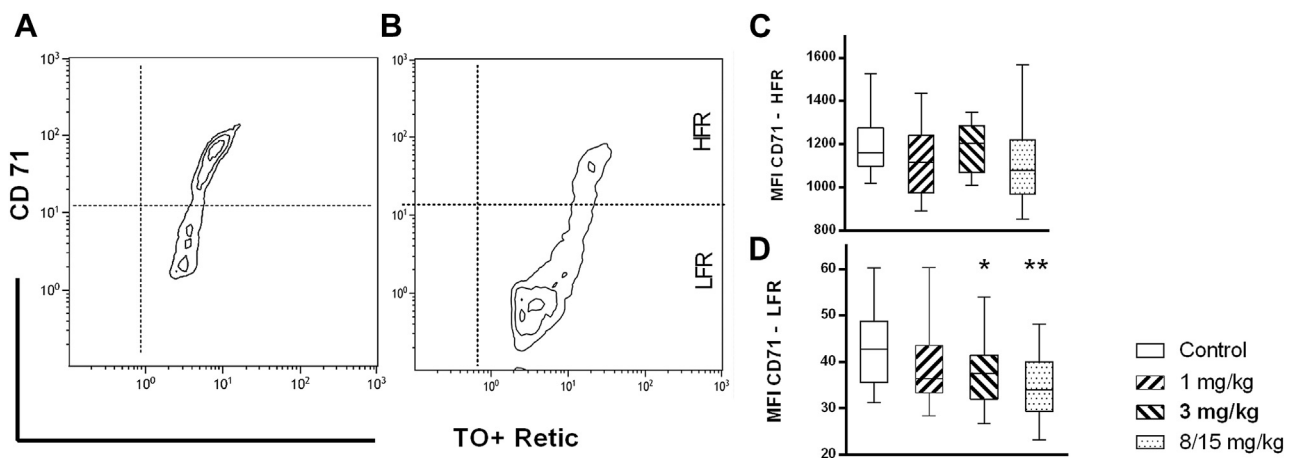


**Figure 5.** GlyT1 inhibition downregulates transferrin receptor expression. Downregulation of TfR-1 expression on reticulocytes indicated reduced iron incorporation into erythroblasts and thus reduced availability of functional iron. Reduction of CD71 expression on reticulocytes at end of treatment is shown by Thiazole orange (TO)–CD71 contour blots on both the immature high fluorescence reticulocytes (HFR) fraction and the more mature low fluorescence reticulocyte fraction (LFR), depicted on two representative animals: control (A) and treated with 15 mg/kg bitopertin (B). A significant reduction in mean group CD71 expression rates at study termination is depicted in the box and whisker blots in (C) and (D). \* $p < 0.05$ , \*\* $p < 0.01$ .

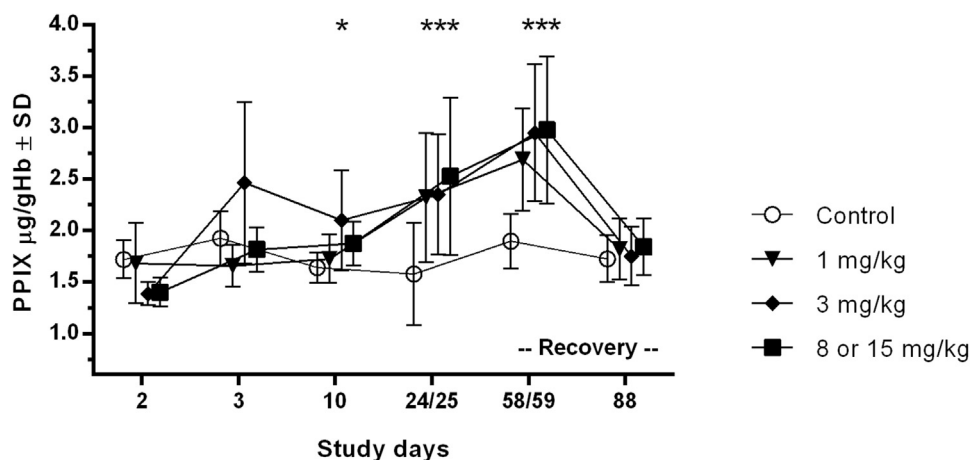


**Figure 6.** GlyT1 inhibition increases total free PPIX. A modest but statistically significant increase in total free erythrocyte PPIX was noted from days 24 and 25 to the end of the treatment period. PPIX then decreased to above control group levels at the end of the treatment period. Mean  $\pm$  SD levels of total free PPIX in the bitopertin dose group measured on day 2 (gavage dosed sub-group;  $n = 4$ ), day 3 (diet admix subgroup;  $n = 4$ ), day 10 (data combined;  $n = 8$ ), days 24/25 (data combined;  $n = 16$ ), at the end of the treatment period (day 58/59, data combined;  $n = 16$ ), and at the end of the recovery period (day 88, data combined;  $n = 12$ ) are shown. \* $p < 0.05$ , \*\*\* $p < 0.001$  in treated groups compared with controls.

reduced availability of functional iron. Downregulation of TfR-1 on erythroblasts and reduced erythroblast iron incorporation has also been reported in GlyT1<sup>-/-</sup> mice [16]. These findings contrast with human data and an animal model considered relevant for human sideroblastic anemia in which TfR-1 expression is significantly upregulated [25,26].

Although IBs are formed by mitochondrial excess of iron, the weak increase in free PPIX observed with GlyT1 inhibition may indicate at the same time a small net deficit of available iron within the erythroblasts, resulting in protoporphyrin not being transformed into heme by ferrochelatase. The most likely explanation is that of a slight

asynchrony between the shutoff of TfR-1 synthesis/iron uptake and the reduction in ALA and protoporphyrin synthesis due to reduced availability of glycine. It is possible that reduced heme synthesis results in an iron-replete signaling within the mitochondria [27], which decreases TfR-1 synthesis and iron uptake but at the same time may result in transient upregulation of ALAS2, producing a small excess synthesis of protoporphyrin above the available iron. Such a paradoxical coexistence of mitochondrial iron accumulation and PPIX increase has also been reported for disorders with a distinct IB pathoetiology, such as refractory anemia with ring sideroblasts [28] and X-linked sideroblastic anemia with ataxia [6]. An iron-deplete signal would be

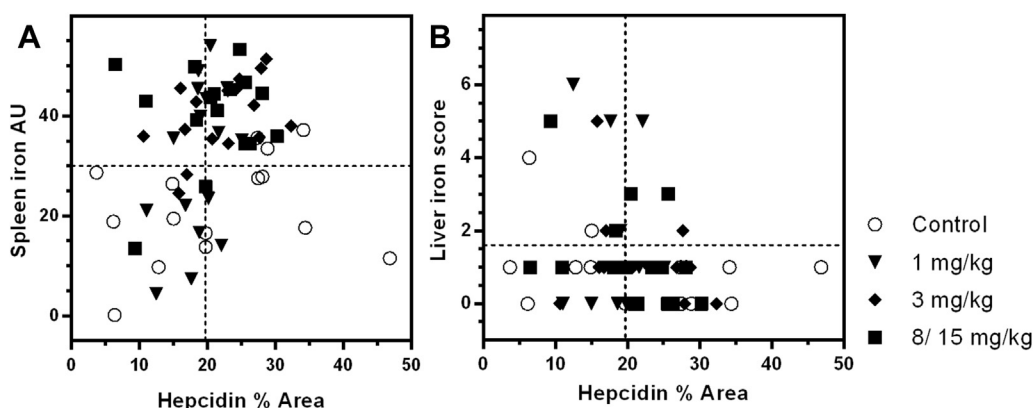


**Figure 7.** Hepcidin as a regulator of iron tissue distribution in the spleen and liver. Correlation analysis of hepcidin expression versus quantitative image analysis of spleen hemosiderin and histology liver iron score at the end of treatment is shown. Although hepcidin expression was not affected under GlyT1 inhibition, hepcidin was a strong regulator of iron tissue distribution within the observed range of expression. Hepcidin expression at the higher range of normal was strongly associated with preferential spleen iron deposition (A). Conversely, an elevated liver iron score was associated with hepcidin expression rates at the lower range of normal (B). The liver–hepcidin correlation has its limitations due to the semiquantitative nature of a histology score, with its low sensitivity and linearity at subtle levels of liver iron depositions. Dotted horizontal lines represent the upper limit of normal from control animals, and the vertical line represents the median of the percentage of control group hepcidin expression.

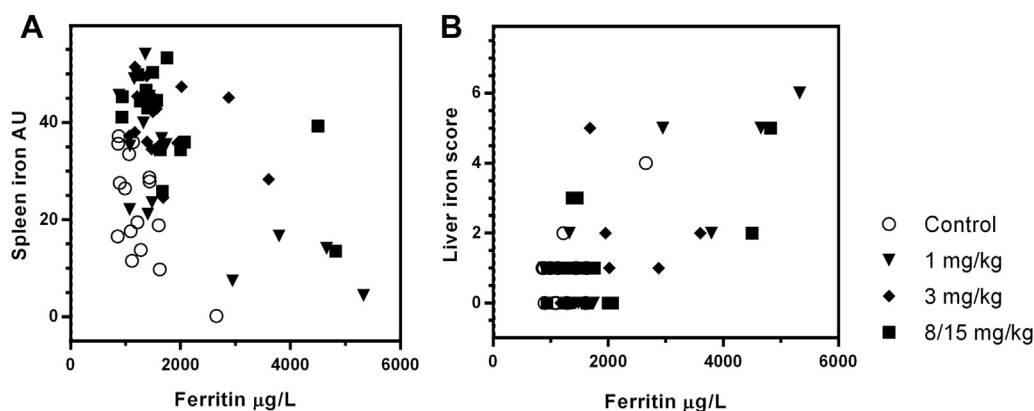


**Figure 8.** Serum ferritin is insensitive for spleen iron accumulation. Correlation analysis of serum ferritin concentrations versus quantitative image analysis of spleen hemosiderin and histology liver iron at the end of treatment is shown. Serum ferritin is insensitive for spleen iron accumulation. At high spleen iron deposition, serum ferritin concentrations are mostly unremarkable (A), whereas elevated liver iron deposition is associated with significantly increased serum ferritin (B).

furthermore consistent with the observed mild thrombocytosis because elevated platelet counts are typically found in iron deficiency anemia, although the molecular activation pathways are unknown [29].

Even though the IBs found in this study showed ultrastructural similarities with IBs of sideroblastic anemia, their rapid and marked formation within 24 hours, their restriction predominantly to reticulocytes, and in particular, the absence of pathological bone marrow sideroblasts render the bitopertin-induced IBs pathogenetically distinct from those associated with acquired forms of sideroblastic anemia. Why IBs are formed under these experimental conditions is incompletely understood, but it can be hypothesized that it is the inability to adapt with an adequate reduction in iron incorporation to the reduced heme biosynthesis, resulting in accumulation of iron in the mitochondria. To date, IBs have not been detected in cynomolgus monkeys and humans treated with bitopertin (unpublished data), pointing to the well-known differences in iron regulation and homeostasis within mammalian species. Significant transcriptome differences during human and murine terminal erythroid differentiation were reported recently [30] and are consistent with older studies showing that, for example, the final heme synthesis rate is higher in rat than in human reticulocytes [31]. Therefore, reduction in heme synthesis induced by inhibition of GlyT1 might cause a higher fraction of remaining uncommitted mitochondrial iron in rat reticulocytes; however, a final proof of this hypothesis is missing.

Although GlyT1 inhibition disturbed Hb synthesis, systemic iron homeostasis remained unaffected. The significant increase in the iron-stained areas, predominantly in the spleen, associated with moderate increases in serum ferritin was observed in treated rats, indicating iron retention. This is due to a shift in iron from the Hb/RBC compartment to the iron storage compartment, also reported for various forms of hyporegenerative anemias [32]. Importantly, critical

organs for tissue iron accumulation, such as the heart and pancreas, were negative for iron/hemosiderin even when rats were treated with bitopertin for 2 years.

Hepcidin expression was not affected under GlyT1 inhibition. Hepcidin downregulation is well documented in conditions of ineffective erythropoiesis and dyserythropoietic anemias, including sideroblastic anemia [33,34]. Systemic iron acquisition under these types of anemia is obviously independent from the status of the existing iron stores (iron overload anemia). The mechanisms by which erythropoietic activity modulates the iron supply remain, however, incompletely understood. A number of mediators released by erythroblasts have been identified as strong co-regulators of hepcidin expression, with significant differences in expression activity between regenerative and ineffective erythropoiesis [33,35]. Hemolytic anemias, even with massive peripheral destruction of erythrocytes such as sickle cell anemia, do not stimulate intestinal iron absorption [36–38] and do not significantly depress hepcidin synthesis, although the regenerative erythropoietic activity is high. However, these conditions are characterized by the absence of ineffective erythropoiesis and thus a significantly lower iron turnover within the erythron. This contrasts to the condition of ineffective erythropoiesis, in which an abnormal rate of apoptosis within maturing erythroblasts causes an overproportionally high intra-marrow iron release and turnover. The regulatory pathways of anemia with systemic iron acquisition are therefore distinct from the conditions seen under the inhibition of GlyT1.

The data also provide experimental evidence about the central regulatory role of hepcidin for iron tissue distribution [39,40]. When hepcidin is high, ferroportin is degraded, iron export from macrophages is blocked, and iron is thus preferentially retained and stored in spleen macrophages [41]. At low hepcidin concentrations, ferroportin transporters are active, iron is exported from macrophages, and iron stores in hepatocytes are activated [42].

Although hepcidin activity was not altered directly by GlyT1 inhibition, hepcidin showed a significant regulatory role in tissue distribution of storage iron when heme biosynthesis and iron reutilization were reduced. Indeed, a preferential spleen but low liver iron deposition was noted in rats under GlyT1 inhibition at hepcidin expression levels at the higher range of normal. In contrast, rats with a comparable increased pool of storage iron but concurrent hepcidin expression rates at the lower range of normal showed elevated liver iron scores but low spleen iron deposition. High serum ferritin concentration correlated preferentially with liver iron deposition, but ferritin was relatively insensitive for spleen hemosiderosis. Because serum ferritin reflects the actual synthesis rate of tissue ferritin and thus steady-state storage iron bioavailability, it is well established that serum ferritin concentration does not accurately reflect total hemosiderin iron stores [43]. This clearly explains the striking discrepancy between the pronounced spleen hemosiderosis and the only modest and statistically insignificant elevation of serum ferritin in this study. The extent to which other confounding factors have interfered in this study with iron regulatory pathways remains unknown. The moderate increase in mean control group serum ferritin, based on abnormal high values in a few individual animals, might point to a recently identified mutation in TfR-2, which has been associated with the sporadically observed iron overload pathology of Wistar rats [44]. Even though the prevalence in the breeding line used here is unknown, such a genetic predisposition might have not only accounted for the observed changes in control animals, but may have also interfered with the GlyT1-induced iron retention, thereby contributing to the interindividual variability of serum ferritin, hepcidin expression, and spleen and liver iron load in treated animals.

This rat study demonstrates that GlyT1 inhibition causes a significant reduction in heme biosynthesis seen as a regenerative hypochromic microcytic anemia. These results also provide robust evidence that GlyT1 inhibition does not cause systemic iron accumulation in rats. Although hepcidin expression was not affected, the results provide an interesting insight into hepcidin-regulated iron tissue distribution, explaining the liver/spleen dichotomy of storage iron. Overall, maximal inhibition of GlyT1 generated a nonprogressive 20% steady-state reduction of MCH, MCV, and Hb, demonstrating that GlyT1 is an essential but nonexclusive glycine transporter in erythroblasts.

An imbalanced heme–globin interregulation leading to excess of either free heme or globin chains is the well-established pathogenesis of a broad spectrum of hematological diseases such as beta-thalassemia or erythropoietic porphyria. Delayed globin transcription with an associated excess of free heme has been identified recently in bone marrow culture systems from patients with Diamond-Blackfan anemia and del(5) myelodysplastic syndrome as the causal reason for the ineffective erythropoiesis [45].

Those studies also provided experimental evidence that inhibition of heme synthesis could improve erythroblast survival. The selective inhibition of heme biosynthesis with an undisturbed systemic iron homeostasis by targeting GlyT1 might provide a promising therapeutic concept for such disorders.

### Acknowledgments

This work was funded by F. Hoffmann-La Roche, Ltd., Basel, Switzerland. Editorial assistance with the preparation of this manuscript was provided by Meridian HealthComms, Ltd., funded by F. Hoffmann La-Roche, Ltd.

M.W., A.K., D.A., and G.S. were responsible for the concept of the study. M.W. and J.F. evaluated all data. F.C. was responsible for assay development and evaluation, A.P. for electron microscopy, and B.A. for in vivo experiments. M.W., J.F., A.K., D.A., and T.S. prepared the manuscript. T.S. supervised the project. All authors critically reviewed and approved the final version of the manuscript.

### Conflict of interest disclosure

All authors except A.P. are employees of F. Hoffmann-La Roche, Ltd.

### References

1. Kim KM, Kingsmore SF, Han H, et al. Cloning of the human glycine transporter type 1: molecular and pharmacological characterization of novel isoform variants and chromosomal localization of the gene in the human and mouse genomes. *Mol Pharmacol.* 1994;45:608–617.
2. King PA, Gunn RB. Na- and Cl-dependent glycine transport in human red blood cells and ghosts: a study of the binding of substrates to the outward-facing carrier. *J Gen Physiol.* 1989;93:321–342.
3. Felipe A, Vinas O, Remesar X. Changes in glycine and leucine transport during red cell maturation in the rat. *Biosci Rep.* 1990;10:209–216.
4. Harvey JW. The erythrocyte: physiology, metabolism and biochemical disorders. In: Kaneko JJ, Harvey JW, Bruss M, eds. *Clinical biochemistry of domestic animals.* San Diego, CA: Academic Press; 1997. p. 157–203.
5. Ajioka RS, Phillips JD, Kushner JP. Biosynthesis of heme in mammals. *Biochim Biophys Acta.* 2006;1763:723–736.
6. Iolascon A, De Falco L, Beaumont C. Molecular basis of inherited microcytic anemia due to defects in iron acquisition or heme synthesis. *Haematologica.* 2009;94:395–408.
7. Skadberg O, Brun A, Sandberg S. Human reticulocytes isolated from peripheral blood: maturation time and hemoglobin synthesis. *Lab Hematol.* 2003;9:198–206.
8. Lee E, Choi HS, Hwang JH, Hoh JK, Cho YH, Baek EJ. The RNA in reticulocytes is not just debris: it is necessary for the final stages of erythrocyte formation. *Blood Cells Mol Dis.* 2014;53:1–10.
9. Ellory JC, Jones SE, Young JD. Glycine transport in human erythrocytes. *J Physiol.* 1981;320:403–422.
10. Ganz T, Nemeth E. Iron metabolism: interactions with normal and disordered erythropoiesis. *Cold Spring Harb Perspect Med.* 2012;2:a011668.
11. Pinard E, Alanine A, Alberati D, et al. Selective GlyT1 inhibitors: discovery of 4-(3-fluoro-5-trifluoromethylpyridin-2-yl)piperazin-1-yl]5-methanesulfonyl-2-((S)-2,2,2-trifluoro-1-methylethoxy)phenyl]methanone (RG1678), a promising novel medicine to treat schizophrenia. *J Med Chem.* 2010;53:4603–4614.

12. Alberati D, Moreau JL, Lengyel J, et al. Glycine reuptake inhibitor RG1678: a pharmacologic characterization of an investigational agent for the treatment of schizophrenia. *Neuropharmacology*. 2012;62:1152–1161.
13. Piomelli S. Free erythrocyte porphyrins in the detection of undue absorption of Pb and of Fe deficiency. *Clin Chem*. 1977;23:264–269.
14. Mufti GJ, Bennett JM, Goasguen J, et al. Diagnosis and classification of myelodysplastic syndrome: International Working Group on Morphology of myelodysplastic syndrome (IWGM-MDS) consensus proposals for the definition and enumeration of myeloblasts and ring sideroblasts. *Haematologica*. 2008;93:1712–1717.
15. Brugnara C, Schiller B, Moran J. Reticulocyte hemoglobin equivalent (Ret He) and assessment of iron-deficient states. *Clin Lab Haematol*. 2006;28:303–308.
16. Schranzhofer M, Bergeron R, Ponka P. Glycine transporter 1 plays a crucial role in hemoglobinization. *Blood*. 2011;118: Abstract 345.
17. Loeffler M, Pantel K, Wulff H, Wichmann HE. A mathematical model of erythropoiesis in mice and rats. Part I: Structure of the model. *Cell Tissue Kinet*. 1989;22:13–30.
18. Djaldetti M, Bergman M, Salman H, Cohen AM, Bessler H. Ultrastructural features of bone marrow cells from patients with acquired sideroblastic anemia. *Microsc Res Tech*. 2004;63:155–158.
19. Sheftel AD, Richardson DR, Prchal J, Ponka P. Mitochondrial iron metabolism and sideroblastic anemia. *Acta Haematol*. 2009;122:120–133.
20. Koc S, Harris JW. Sideroblastic anemias: variations on imprecision in diagnostic criteria, proposal for an extended classification of sideroblastic anemias. *Am J Hematol*. 1998;57:1–6.
21. Griffiths RE, Kupzig S, Cogan N, et al. Maturing reticulocytes internalize plasma membrane in glycophorin A-containing vesicles that fuse with autophagosomes before exocytosis. *Blood*. 2012;119:6296–6306.
22. William BM, Thawani N, Sae-Tia S, Corazza GR. Hyposplenism: a comprehensive review. Part II: clinical manifestations, diagnosis, and management. *Hematology*. 2007;12:89–98.
23. Ermens AA, Otten R. Pappenheimer bodies in a splenectomized patient with alcohol abuse. *Blood*. 2012;119:3878.
24. De Haan LD, Werre JM, Ruben AM, Huls AH, de Gier J, Staal GE. Reticulocyte crisis after splenectomy: evidence for delayed red cell maturation? *Eur J Haematol*. 1988;41:74–79.
25. Nakajima O, Okano S, Harada H, et al. Transgenic rescue of erythroid 5-aminolevulinic synthase-deficient mice results in the formation of ring sideroblasts and siderocytes. *Genes Cells*. 2006;11:685–700.
26. Metzgeroth G, Rosee PL, Kuhn C, et al. The soluble transferrin receptor in dysplastic erythropoiesis in myelodysplastic syndrome. *Eur J Haematol*. 2007;79:8–16.
27. Huang ML, Lane DJ, Richardson DR. Mitochondrial mayhem: the mitochondrion as a modulator of iron metabolism and its role in disease. *Antioxid Redox Signal*. 2011;15:3003–3019.
28. Cuijpers ML, Raymakers RA, Mackenzie MA, et al. Recent advances in the understanding of iron overload in sideroblastic myelodysplastic syndrome. *Br J Haematol*. 2010;149:322–333.
29. Evstatiev R, Bukaty A, Jimenez K, et al. Iron deficiency alters megakaryopoiesis and platelet phenotype independent of thrombopoietin. *Am J Hematol*. 2014;89:524–529.
30. An X, Schulz VP, Li J, et al. Global transcriptome analyses of human and murine terminal erythroid differentiation. *Blood*. 2014;123:3466–3477.
31. Verhoef NJ, Noordeloos PJ, Leijnse B. Heme synthetase activity in normal human and rat erythroid cells and in sideroblastic anemia. *Clin Chim Acta*. 1978;82:45–53.
32. Adams PC, Barton JC. A diagnostic approach to hyperferritinemia with a non-elevated transferrin saturation. *J Hepatol*. 2011;55:453–458.
33. Tanno T, Miller JL. Iron loading and overloading due to ineffective erythropoiesis. *Adv Hematol*. 2010;2010:358283.
34. Ganz T, Nemeth E. Regulation of iron acquisition and iron distribution in mammals. *Biochim Biophys Acta*. 2006;1763:690–699.
35. Kautz L, Jung G, Valore EV, Rivella S, Nemeth E, Ganz T. Identification of erythroferrone as an erythroid regulator of iron metabolism. *Nat Genet*. 2014;46:678–684.
36. Mariani R, Trombini P, Pozzi M, Piperno A. Iron metabolism in thalassemia and sickle cell disease. *Mediterr J Hematol Infect Dis*. 2009;1:e2009006.
37. Andrews NC. A genetic view of iron homeostasis. *Semin Hematol*. 2002;39:227–234.
38. Kearney SL, Nemeth E, Neufeld EJ, et al. Urinary hepcidin in congenital chronic anemias. *Pediatr Blood Cancer*. 2007;48:57–63.
39. Viatte L, Nicolas G, Lou DQ, et al. Chronic hepcidin induction causes hyposideremia and alters the pattern of cellular iron accumulation in hemochromatotic mice. *Blood*. 2006;107:2952–2958.
40. Langdon JM, Yates SC, Femnou LK, et al. Hepcidin-dependent and hepcidin-independent regulation of erythropoiesis in a mouse model of anemia of chronic inflammation. *Am J Hematol*. 2014;89:470–479.
41. Pak M, Lopez MA, Gabayan V, Ganz T, Rivera S. Suppression of hepcidin during anemia requires erythropoietic activity. *Blood*. 2006;108:3730–3735.
42. Ganz T. Cellular iron: ferroportin is the only way out. *Cell Metab*. 2005;1:155–157.
43. Saito H, Tomita A, Ohashi H, Maeda H, Hayashi H, Naoe T. Determination of ferritin and hemosiderin iron in patients with normal iron stores and iron overload by serum ferritin kinetics. *Nagoya J Med Sci*. 2012;74:39–49.
44. Bartnikas TB, Wildt SJ, Wineinger AE, et al. A novel rat model of hereditary hemochromatosis due to a mutation in transferrin receptor 2. *Comp Med*. 2013;63:143–155.
45. Yang Z, Keel SB, Shimamura A, et al. Delayed globin synthesis leads to excess heme and the macrocytic anemia of Diamond Blackfan anemia and del(5q) myelodysplastic syndrome. *Sci Transl Med*. 2016;8:338ra367.

## Supplementary methods

### *Study design and procedures: long-term studies of GlyT1 inhibition*

Female Wistar rats were exposed to bitopertin at daily doses of 0, 1, 3, 10, or 15 mg/kg for 6 months ( $n = 26$  per group, dosed by oral gavage) and daily doses of 0, 1, 3, or 8 mg/kg for 2 years ( $n = 72$  per group, dosed by diet admix). Hematology samples were taken throughout the study period; at week 7, 14, and 27 in a subgroup ( $n = 10$ ) from the 6-month study; and at week 48 and terminal necropsy in a subgroup ( $n = 12$ ) from the 2-year study. Histopathology of organs and tissues was conducted in all animals at the end of the dosing period.

Blood smears were evaluated in the 2-year exposure study. A less detailed IB-grading system was applied than in the 8-week study, in which the presence of IBs was noted with additional information as to whether IBs are predominantly present in polychromatic (immature) or mature RBCs.

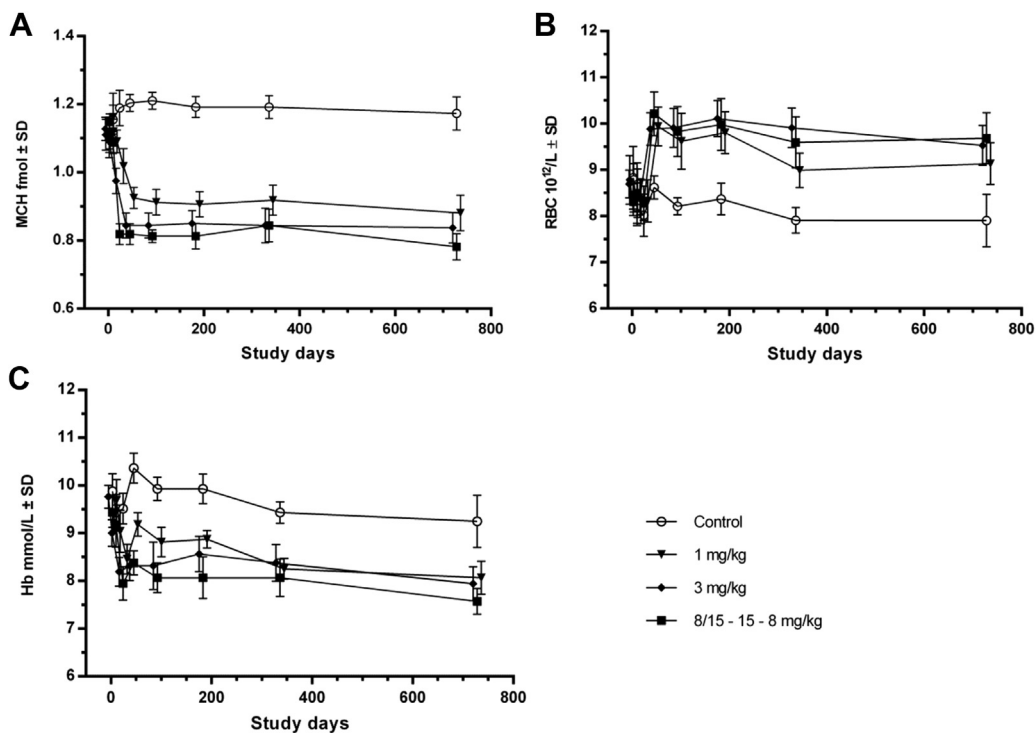
*HAMP expression in the liver by in situ hybridization.* The left lateral lobe of the liver was sampled at necropsy and embedded in paraffin. Formalin-fixed and paraffin-embedded tissue sections (3–4  $\mu\text{m}$  thick) were deparaffinized and treated with protease according to the manufac-

turer's instructions. A mixture of HAMP-specific RNA target probe sets for the rat was provided by the manufacturer (Entrez Gene ID 84604, targeted bps 50–322 of the HAMP cDNA sequence). After signal amplification, slides were stained with Fast Red and counterstained with hematoxylin. All steps of this procedure were performed using an immunostainer (Ventana Discovery Ultra®, Ventana Medical System, Tucson, AZ). Probes to the bacterial gene *dapB* and the endogenous *Ubc* mRNA were used as negative and positive controls, respectively, for each case. Specific staining signals were identified as red, punctate dots present in the cytoplasm.

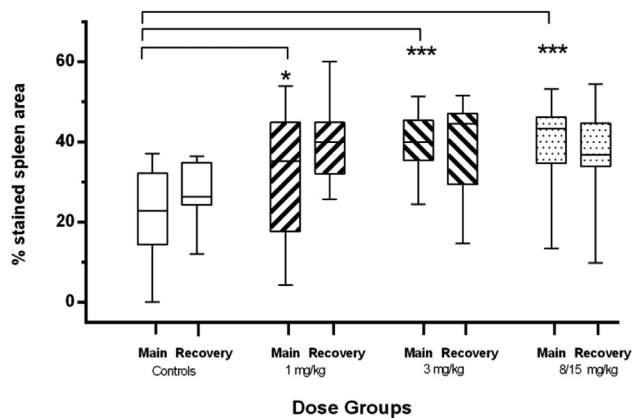
Stained slides from all animals were scanned with the AperioAT® full-slide scanner and image analysis was performed using the Definiens TissueStudio® software version 3.51. The relative stained area from the whole liver tissue section was calculated.

### *Imaging of spleen iron*

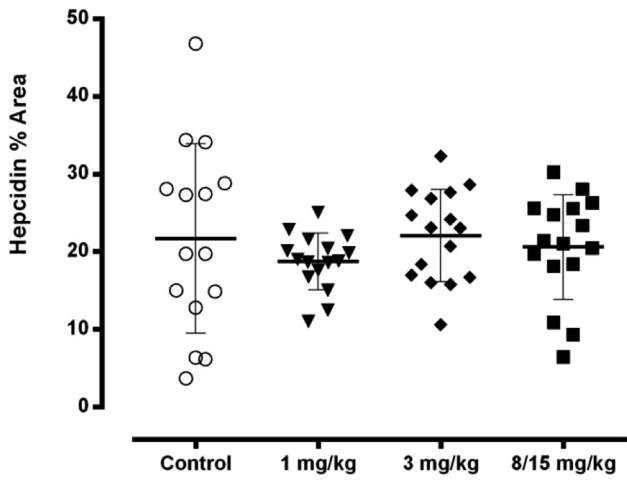
Automated image analysis for iron was performed on Perls' stained spleen slides by scanning with a full-slide scanner (AperioAT®, Aperio Technologies, Inc., Vista, CA) and analysis with Definiens TissueStudio® version 3.51 software (Definiens AG, Munich, Germany). The relative iron-stained area (hemosiderin deposits) was calculated as a percentage of the total spleen area.



**Supplementary Figure E1.** Chronic exposure to bitopertin causes steady-state microcytic hypochromic erythropoiesis. Hematology parameters (mean  $\pm$  SD) by dose group in long-term studies of bitopertin treatment in rats are shown. Figures represent composite data from female rats in this study (up to day 24) and from the 6-month study (days 45–183) and 2-year study (days 336–728). Once the exposure duration has exceeded one RBC lifespan (approximately 60 days), bitopertin results in steady-state microcytic hypochromic erythropoiesis with stable and nonprogressive elevations of RBCs (A), a reduction in MCH (B), and a total reduction in Hb (C). An equipotent effect on heme synthesis was seen at high-dose exposure ranges at 8–15 mg/kg in all three combined studies, indicating a maximal inhibitory effect on GlyT-1 function with bitopertin.



**Supplementary Figure E2.** Spleen iron retention. Box-and-whisker plots showing percentage iron-stained spleen area by dose group measured by imaging at the end of the treatment (main) period and the end of the recovery period. Iron deposition was significantly increased in all groups at the end of the treatment period and was only insignificantly reversed during the 28-day recovery period due to the relative low bioavailability of hemosiderin iron. Statistical significance tested for the end of treatment phase: \* $p < 0.05$ , \*\*\* $p < 0.001$ .



**Supplementary Figure E3.** GlyT1 inhibition does not affect hepcidin expression. Hepcidin expression was not affected under GlyT1 inhibition. Mean group and individual levels of hepatic hepcidin expression at the end of the treatment period by dose group are shown.